E2SWITCH
Energy Efficient Tunnel FET Switches and Circuits

Co-funded by the European Union

E²SWITCH

Energy Efficient Tunnel FET Switches and Circuits

Grant Agreement No.: 619509

Funding Scheme: Collaborative project

Thematic Area: Energy efficient switch, tunnel FET, nanotechnology III-V, SiGe and Ge, low power integrated circuits, digital and analog/RF circuits, CMOS, simulation and modeling of nano-electronic devices & circuits

Project start date: 01-11-2013

Deliverable D3.1	**Calibrated band-to-band tunnelling models in Sentaurus-Device for Si/SiGe, Si/III-V, and all-III-V TFETs**

Nature[1]**:** R

Dissemination level[2]**:** PU

Due date[3]**:** M09

Date of delivery: M10

Lead partner: ETHZ

Contributing partners: IUNET

Authors: S. Sant, H. Carrillo-Nunez, M. Luisier, A. Schenk (ETHZ), D. Esseni, P. Osgnach, P. Palestri, A. Revelant, L. Selmi, S. Strangio (IUNET)

---

[1] R = Report, P = Prototype, D = Demonstrator, O = Other

[2] PU = Public, PP = Restricted to other programme participants (including the Commission Services, RE = Restricted to a group specified by the consortium (including the Commission Services), CO = Confidential, only for the members of the consortium (including the Commission Services)

[3] Measured in months from the project start date (M01)

Revision history

Version	Date	Author	Comment
0.1	26-07-2014	A. Schenk	First draft
1.0	11-08-2014	A. Ionescu, K. Leufgen	Final version, formally revised and approved by AI

Point of Contact[4]**:**

Prof. Dr. Andreas Schenk, ETHZ

schenk@iis.ee.ethz.ch

+41 44 632-6689

[4] For up-to-date contact details, please refer to the contact page of the Members section: http://www.E2SWITCH.org/members/contactdetails/index.php.

Contents

SUMMARY 4

1 INTRODUCTION 5

2 CALIBRATION OF THE FULL-BAND QUANTUM-TRANSPORT SIMULATOR OMEN OF ETHZ AND PARAMETER EXTRACTION FOR S-DEVICE 6

2.1 PHYSICAL MODEL 6
2.2 TB PARAMETERS AND VALIDATION 6
2.3 TCAD PARAMETER CALIBRATION USING OMEN SIMULATIONS OF ESAKI DIODES 7

3 TCAD TOOL SENTAURUS-DEVICE CALIBRATED ON 30 BAND K·P RESULTS 10

3.1 SIMULATION OF SIGE HETEROSTRUCTURE 10
3.1.1 MODEL 10
3.1.2 DEVICE STRUCTURES 10
3.2 CALIBRATION RESULTS 12
3.3 FUTURE WORK 14

4 TCAD TOOL SENTAURUS-DEVICE CALIBRATED ON S-BAND (SYNOPSYS) 15

4.1 PSEUDOPOTENTIAL CALCULATIONS OF GROUP-IV (SI, GE, AND SN) ALLOYS 15
4.2 SIMULATION OF HETERO-STRUCTURE TUNNEL FETS 17
4.3 FUTURE WORK 18

5 CONCLUSION 19

REFERENCES 20

Summary

We report on the derivation of an accurate set of band-to-band tunnelling (BTBT) parameters, that can be applied to a wide range of Tunnel FET (TFET) configurations and that properly accounts for the material properties of various semiconductors (Si, Ge, III-V, GeSn, Si-InAs, GaSb-InAs). The calibration was done in a hierarchical way starting with the ad-hoc simulators OMEN (full-band, NEGF) and a 30 band k•p electronic structure calculator. These ad-hoc simulators were then used to extract the necessary parameters (density of states, effective masses, band gaps, band offsets, and effective tunnel gaps) for the implemented BTBT models in the commercial device simulator Sentaurus-Device (S-Device) which serves as the work horse for the comprehensive simulation studies of the TFETs fabricated in the project.

The tight-binding parameters in OMEN have been optimized to reproduce the complete bulk band structure of semiconductors including all materials covered in the project. Technology-computer-aided-design (TCAD) calibrations by comparison with OMEN results were based on short (ballistic) homo- and hetero Esaki diodes, suppressing the dissipative effects in S-Device. In the case of InAs-Si hetero-junctions it was found that the inter-material tunnelling is a direct (zero-phonon) process. Two TCAD variants have been discussed to match this case. The parameters of the non-local dynamic path BTBT model (Kane model) in S-Device were also adjusted based on the band structure information obtained with a 30 band k•p model. In particular, the parameters *A* and *B* of Kane's two-band model contain the effective masses and the band gap that have been extracted from the 30 band k•p model for Si and SiGe.

The nonlocal Empirical Pseudo-potential Method (EPM) was applied to generate band structure parameters for the calibration of the Kane model in S-Device using the tool S-Band of Synopsys. This was done for the group-IV element alloys, Si, Ge, and Sn. The band structures of GeSn and SiGeSn were calculated by employing the Virtual Crystal Approximation. The local EPM parameters for the alloy of any given composition were obtained by linearly interpolating the local EPM parameters of the individual atoms. The variation of lattice constants of GeSn and SiGeSn with the alloy composition was modelled using quadratic expressions fitted to the experimental lattice constants. The application in 3D simulation of SiGe/Si TFETs fabricated by the project partner FZJ (Jülich) was demonstrated. It was found that the presence of strain in the SiGeSn layer doesn't change the sub-threshold characteristics much but reduces the on-state current.

1 Introduction

Device simulation can help predict the behaviour of not-yet fabricated tunnel devices and accelerate the innovation of novel, highly efficient TFET architectures. For this, a fast technology computer aided design (TCAD) tool that provides accurate band-to-band tunnelling (BTBT) rates, that can treat a wide range of TFET configurations (lateral vs. vertical tunnelling, 2D vs. 3D structures, non-symmetrical gate contacts), and that properly accounts for the material properties of various semiconductors (Si, Ge, III-V, GeSn, Si-InAs, GaSb-InAs) is needed. Furthermore, when BTBT occurs across a hetero-junction such as Si-InAs, Si-SiGe, or GaSb-InAs, a physics-based extension of the models is needed that (i) accounts for band structure mismatch and lattice-induced strain at the material interfaces, (ii) uses the correct complex band dispersion to describe the wave function attenuation caused by tunnelling, (iii) computes numerically the resulting action integrals, (iv) provides direction-dependent tunnelling probabilities, and (v) includes band gap narrowing as fitting parameter. A conventional TCAD tool must be calibrated first with more advanced simulation approaches, otherwise its results might have very limited predictive meaning.

The calibration is done in a hierarchical way starting with the ad-hoc simulators OMEN (full-band, NEGF) and a 30 band k·p electronic structure calculator which are validated on experimental data and band structure parameters generated by DFT tools. These ad-hoc simulators are then used to extract the necessary parameters (density of states (DOS), effective masses, band gaps, band offsets, effective tunnel gaps) for the implemented BTBT models in the commercial device simulator Sentaurus-Device which serves as the work horse for the comprehensive simulation studies of the TFETs fabricated in the project. Therefore, we report here on the

• calibration (validation) of the full-band and atomistic quantum transport simulator OMEN of ETHZ and the calibration of TCAD parameters based on OMEN simulations,

• calibration of the commercial TCAD tool Sentaurus-Device of Synopsys on the k·p band calculations of IUNET,

• calibration of the commercial TCAD tool Sentaurus-Device of Synopsys on the pseudo-potential simulator S-Band.

The calibration on ad-hoc tools is accompanied by comparisons with available experimental data from the project and from literature.

2 Calibration of the full-band quantum-transport simulator OMEN of ETHZ and parameter extraction for S-Device

This section describes the calibration (validation) of the atomistic full-band quantum transport solver OMEN of ETHZ which is based on different flavours of the nearest-neighbour tight-binding (TB) method (sp3s* and sp3d5s*, with and without spin-orbit coupling) and on the Non-equilibrium Green's Function (NEGF) formalism. In the project, OMEN serves as ad-hoc reference tool for the calibration of tunnel parameters to be used in Sentaurus-Device. It will also be directly applied to simulate Si/SiGe, Si/III-V, and Ga(As)Sb/ In(Ga)As hetero-junction Esaki diodes as fabricated in WP1 and characterized in WP2.

2.1 Physical model

OMEN [Lui06] is a state-of-the-art, massively parallel, multi-dimensional, and atomistic quantum transport solver used by more than 1000 individuals worldwide. It has been applied to a variety of TFET materials and designs: III-V single- and double-gate ultra-thin-bodies as well as gate all-around nanowires [MLu09], InAs, Si, and Ge nanowires with phonon-assisted tunnelling [Lui10], planar and 3D InSb, graphene, and GaSb-InAs broken gap hetero-structures [Lui09], 2D TFET architectures with vertical instead of lateral tunnelling paths [Aga10], and InGaAs, bulk-like, Esaki diodes [Cho12]. While OMEN offers a unique palette of TFET configurations that can be treated at a quantum mechanical level, its computational burden is large as compared to Sentaurus-Device, thus preventing the exploration of large design spaces.

In the NEGF formalism, the following quantum transport equations are solved in OMEN for electrons

$$[E - H - \Sigma^{RB}(E) - \Sigma^{RS}(E)] \cdot G^{R}(E) = I$$
$$G^{\gtrless}(E) = G^{R}(E) \cdot [\Sigma^{\gtrless B}(E) + \Sigma^{\gtrless S}(E)] \cdot G^{A}(E) \quad (1)$$

and for phonons

$$[\omega^2 - \Phi - \Pi^{RB}(\omega) - \Pi^{RS}(\omega)] \cdot D^{R}(\omega) = I$$
$$D^{\gtrless}(\omega) = D^{R}(\omega) \cdot [\Pi^{\gtrless B}(\omega) + \Pi^{\gtrless S}(\omega)] \cdot D^{A}(\omega). \quad (2)$$

In Eqs. (1) and (2), G and D are the electron and phonon Green's Functions, that can be retarded (R), advanced (A), lesser ($<$), or greater ($>$), while Σ and Π refer to the corresponding self-energies. The electron (phonon) properties depend on the energy (frequency) E (ω) and on the characteristics of the Hamiltonian (dynamical) matrix H (Φ). The index B stands for boundary and S for scattering (electron-phonon and phonon-phonon). A recursive Green's Function (RGF) algorithm can be used to efficiently solve Eqs. (1) and (2) [Lak97]. The values of Σ^{S} and Π^{S} determine the transport regime under which the device operates. In a scattering scheme with equilibrium phonons the self-energy Π^{S} is set to 0, but not Σ^{S},

$$\Sigma^{S}(E) \propto \Sigma_i V_i^{e-ph} \cdot \nabla H \cdot [n(\omega_i) \cdot G(E + \hbar\omega_i) + (n(\omega_i) + 1) \cdot G(E - \hbar\omega_i)] \cdot \nabla H, \quad (3)$$
$$\Pi^{S}(\omega) = 0, \quad (4)$$

and electron-phonon scattering is turned on: electrons can gain or lose energy by absorbing or emitting phonons, but the phonon population remains at equilibrium and is homogeneously distributed. In Eq. (3), V^{e-ph} is a form factor [LuK09], ∇H the derivative of the Hamiltonian matrix with respect to atomic bond variations, and $n(\omega_i)$ refers to the Bose-Einstein distribution function of phonons with frequency ω_i.

2.2 TB parameters and validation

The TB parameters in OMEN are optimized to reproduce the complete bulk band structure of semiconductors [Jan98, Boy02, Boy04] including all materials covered in the project. For details of the parameter fitting see Refs. [Boy02, Boy04]. The transition from infinite bulk to confined structures is computationally straight-forward. For example, nanowires are constructed by translating their primitive unit cell across the device volume. The atomic on-site energies as well as the connections to the nearest neighbors are modeled with the bulk material parameters, and surface atoms are "passivated" by increasing the dangling-bond energy [Lee04]. The TB model automatically accounts for the imaginary band dispersion that exists in the energy band gap. BTBT processes are therefore accurately modeled for direct gap materials even in the absence of scattering. Tight-binding parameters for InAs and GaAs can be found in Ref. [Boy02].

An accurate description for $In_xGa_{1-x}As$ is possible by introducing bowing parameters for each on-site and two-center integral TB parameters [MLu09] resulting in the widely accepted band gaps and effective masses of the ternary alloys [ioffe]. For hetero tunnel devices the band offsets at the material interface are taken from literature.

Figure 1 shows a comparison between an OMEN simulation of an InAs/GaSb hetero Esaki diode and experimental data [Paw12].

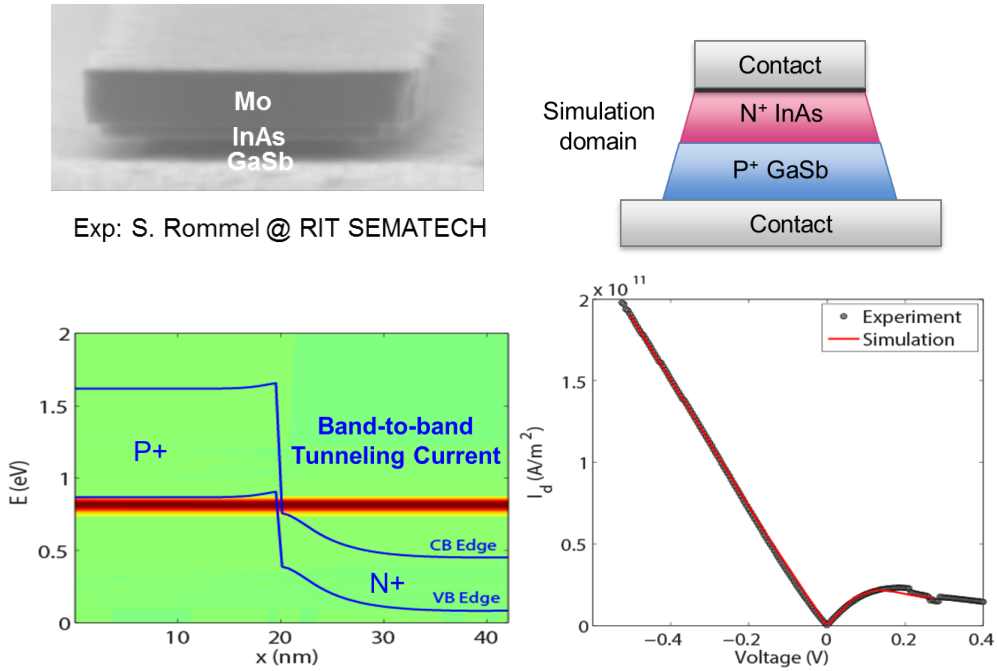

Figure 1: Upper: SEM and sketch of an InAs/GaSb hetero Esaki diode. Lower: OMEN simulation of the spectral current and the IV characteristics in comparison with the measured current [Paw12].

2.3 TCAD parameter calibration using OMEN simulations of Esaki diodes

The BTBT current of short, unconfined Esaki homo diodes (⟨111⟩, 20 nm length, abrupt doping) was simulated with OMEN for different materials and doping levels. For the direct materials (InAs, GaSb) and for Ge, where coherent BTBT is dominant [Lui10], the simulation of bulk diodes is straightforward. Bulk simulations are needed because there is also no geometrical confinement in the fabricated nanowire TFETs (diameters in the range 25 nm – 100 nm). Figure 2 shows that InAs has the highest BTBT current density, followed by GaSb and Ge. The upper limit for InAs is $\sim 5 \times 10^4$ kA/cm^2. In the case of Si, due to the demanding electron-phonon coupling, at least one-dimensional confinement is necessary in the simulation (the direction of confinement is ⟨-110⟩ and periodic continuation was applied in ⟨11-2⟩ direction). The bulk limit of Si remains below 100 kA/cm^2, a factor 500 smaller than that of InAs. Figure 3 presents the comparison between OMEN and S-Device simulations of InAs Esaki diodes using the calibrated TCAD model.

For hetero-structures, the applicability of analytical BTBT models like the "dynamical nonlocal path BTBT" (Kane model) [SDe] might be called into question because no analytical theory/model exists for BTBT between a direct (InAs) and an indirect (Si) semiconductor. A very simple work-around is either to consider a zero-phonon (direct BTBT) or a phonon-assisted (indirect BTBT) tunnelling path through the interface of the two materials as required by S-Device. In an InAs-Si hetero-structure the first case is more appropriate and can be achieved by using the Kane model as given for the InAs side with the well-established values for gap and effective masses, but with calibrated parameters (called "A" and "B" in S-Device) for the silicon side using the experimental data of Solomon et al. [Sol04]. It is labelled "TCAD, bulk parameters" in Figure 4 because the parameters of the bulk materials are applied piecewise. Note that the described complication only occurs for inter-material tunnelling ("point tunnelling") but not for under-the-gate tunnelling ("line tunnelling"). The latter has tunnelling paths fully contained in InAs and dominates the ON-current in a bulk-like InAs-Si TFET.

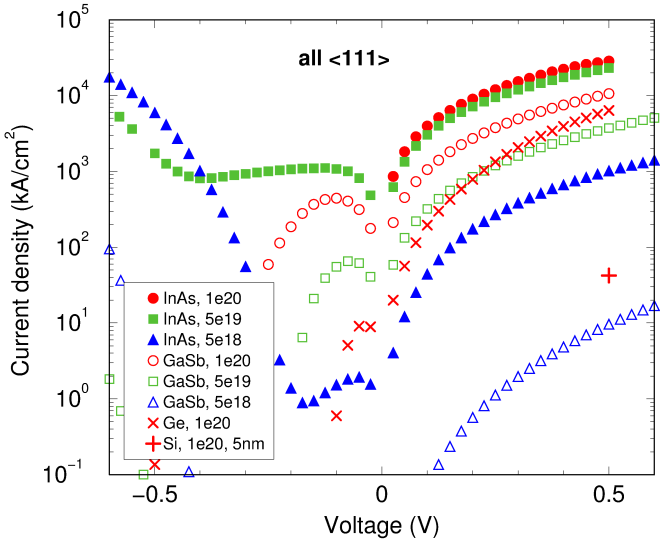

Figure 2: Short Esaki (bulk) diodes with symmetrical doping simulated with OMEN. The single data point for Si was obtained for a 5 nm slab and took 5 h on Jaguar Cray XK6 using ~ 20'000 CPUs. [Sch12].

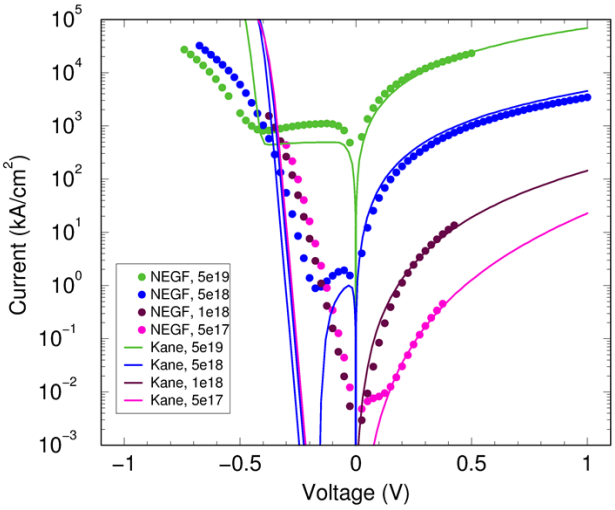

Figure 3: IV characteristics of short InAs homo diodes with symmetrical doping obtained with Kane dispersion in Sentaurus-Device [Sch12]. Comparison between OMEN and S-Device shows good agreement in the high-doping (high-field) range.

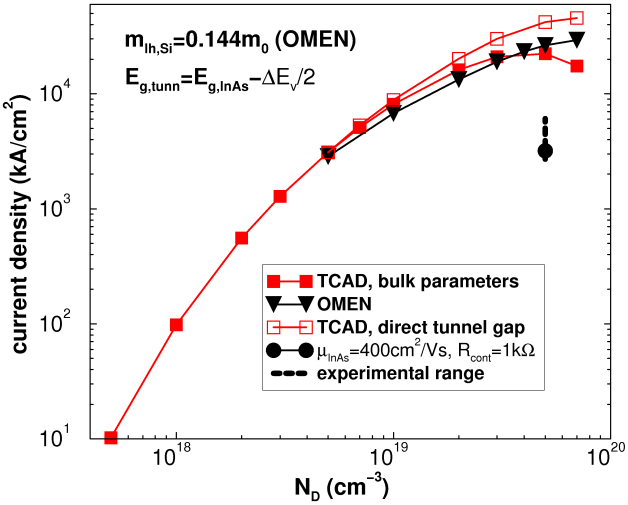

Figure 4: BTBT current density of a bulk-like InAs-Si Esaki diode as a function of donor concentration in InAs at a reverse bias of V = -0.5V . Comparison between OMEN and different TCAD approaches (S-Device) [Nun14].

Assuming that inter-material tunnelling only occurs between the Si valence band and the InAs conduction band, BTBT in the InAs-Si hetero-structure is expected to be mainly direct. This is illustrated in Figure 4 where the ON-current density of a bulk-like InAs-Si Esaki diode (circular geometry, *n*-type InAs nanowire with radius of R ≈ 60 nm grown on a *p*-type ⟨111⟩ Si substrate) is plotted as a function of donor concentration. It has been verified that the tunnelling current computed with OMEN does not depend on the presence of electron-phonon scattering, indicating that the inter-material tunnelling through a Si-InAs junction is direct. It can also be observed in Figure 4 that the ballistic S-Device current simulated by the aforementioned work-around (labelled "TCAD, bulk parameters") agrees well with OMEN up to a concentration of $N_D \approx 4 \times 10^{19}$ cm^{-3}. For higher donor concentrations the pn-junction becomes one-sided. Therefore, the tunnelling path more and more penetrates into Si leading to a decreasing tunnel current since the BTBT rate in bulk silicon is much smaller than that of InAs. This behaviour is not found with OMEN! The discrepancy is a clear indication for direct tunnelling. The direct tunnelling process can be modelled in S-Device using a "model semiconductor", i.e. a homo-junction with a common gap (called "tunnel gap") and a reduced effective mass built from the Si light-hole mass and the InAs Gamma mass. The Si light-hole mass in ⟨111⟩-direction was extracted from OMEN, and the tunnel gap was chosen as the InAs gap reduced by half of the valence band offset (Ev = 80 meV). This results in the open symbols in Figure 4. With such an

approach the current does not drop anymore. Unfortunately, this method cannot be easily applied to hetero TFETs as it would require to identify three types of tunnel paths - bulk-InAs, bulk-Si, and inter-material - each with its own model. Finally, TCAD allows to include the measured mobility in the InAs wires as well as the measured contact resistance. These parasitic resistances have a strong effect on the ON-current as shown in Figure 4 by the single simulation point in comparison with the experimental range.

3 TCAD tool Sentaurus-Device calibrated on 30 band k·p results

This section reports on the methodology used by IUNET-Udine to simulate SiGe based homo- and hetero-junction TFETs. The methodology was developed in a former EU project (STEEPER) and it is here extended to consider different tunnelling path directions. The parameters of the BTBT model of the commercial TCAD simulator Sentaurus-Device of Synopsys are adjusted based on the band structure information obtained with a 30 band k·p model [Rid06]. Examples of application to devices fabricated by the project partner FZJ (Jülich) are provided.

3.1 Simulation of SiGe heterostructure

3.1.1 Model

The non-local dynamic path BTBT model [SDe] has been employed here. As for phonon-assisted BTBT (the dominant mechanism in SiGe TFETs), beside the phonon energy, that is set to 19 meV in Silicon [SDe] and 13.8 meV in $Si_{0.5}Ge_{0.5}$ (linear interpolation between the Si and Ge values in [SDe]), the other model parameters are the terms A and B of Kane's formula. These terms contain information such as effective masses and energy gap that are extracted from the 30 band k·p model for Si and SiGe presented in [Rid06,Liz12]. In particular, we have:

$$A = \frac{g(m_v m_c)^{3/2}(1+2N_{op}){D_{op}}^2(q{F_0}^{5/2})}{2^{21/4}h^{5/2}{m_r}^{5/4}\rho\varepsilon_{op}\,E_G^{7/4}}$$

$$B = \frac{2^{7/2}\pi m_r^{1/2}E_G^{3/2}}{3qh}$$

where the meaning of the parameters can be found in [SDe]. The ones affected by our calibration are E_G, the energy band gap and $m_r = (m_h^{-1}+m_e^{-1})^{-1}$, the reduced mass. The k·p energy band gap is adjusted by considering band gap narrowing according to the model in [Jai90]. The parameters m_e and m_h are the effective masses computed in the transport direction by regression of the non-parabolic analytic dispersion relation

$$E(k,\theta) = \frac{1}{2\alpha(\theta)}\left(-1+\sqrt{1+\frac{2\alpha(\theta)\hbar^2k^2}{m(\theta)}}\right)$$

The terms *A* and *B* are computed for all possible BTBT transitions, i.e. between light or heavy hole band to the different minima of the conduction band. Different simulations are run for each case and then the currents are summed, assuming that the current is so low that the electrostatics is the same for all cases. Results using this approach have been presented in [Rev13]. Here the methodology is applied to the experimental devices presented in [Ric13].

3.1.2 Device structures

Two device architectures have been considered. The first one is the device sketched in Figure 5. Source (drain) constant doping levels of $2{\cdot}10^{20}$ cm^{-3} and abrupt junctions have been assumed. No gate oxide overlap/underlap to the source and drain has been considered. Since the channel is undoped, point tunnelling at the source/channel interface inside the strained SiGe region is dominant. For his reason in the following we denote this template as "homo-junction" even if both Si and SiGe layers are present. Full 3D simulations are very demanding from the computational point of view, so we calculated the current for 2D cuts as indicated in the figure, thus making the implicit assumption that the device is uniform perpendicular to the cut plane. The total drain current was then computed by a linear combination of the weighted output current densities from the 2D structures, obtained by multiplying each 2D current density [A/um] by the width of the nanowire (vertical cut C1 in Figure 5) or by the height of the related layer (horizontal cuts C2 and C3 in Figure 5).

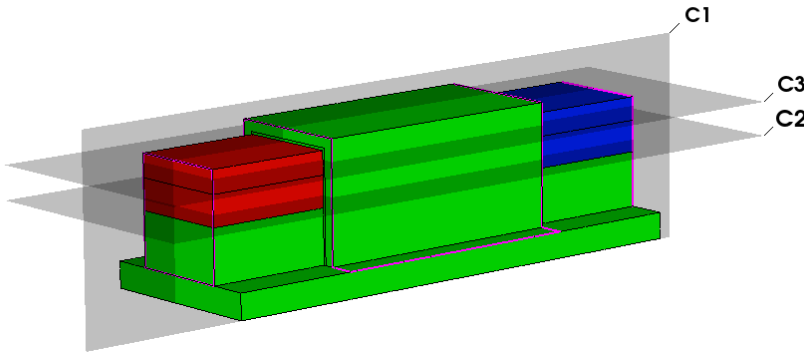

Figure 5: Sketch of the homo-junction device from [Ric13]. Green volumes are oxide or intrinsic Si (or SiGe). Blue indicates p++ doping, red n++. The material stack consists of silicon/SiGe/Si. The region below the gate is undoped.

The second device is sketched in Figure 6. The SiGe layer under the gate is p+ doped as at the source. The device exhibits line tunnelling (vertical) in the region below the gate between the p+ doped SiGe layer and the silicon. Since generation is almost constant along the channel, a full 3D simulation is not needed. Therefore, we consider a 2D mesh corresponding to the section C1 in Figure 6 with the drain contact placed at the bottom and the source contact placed between the p+ SiGe layer and the Si-cap.

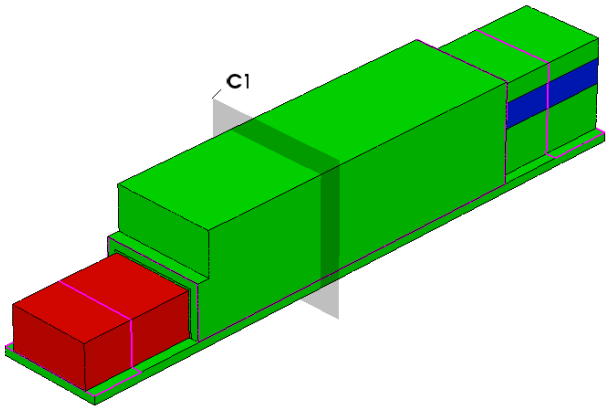

Figure 6: Sketch of the hetero-junction device from [Ric13], same colors as in Figure 5. It consists of 3 layers (bottom to top): Si, p+SiGe and a Si cap. The SiGe is doped also below the gate, whereas the bottom Si layer is doped only in the drain (red region).

Since both devices include different materials (Si and strained SiGe) with different doping levels (hence, different gap due to band gap narrowing), the extraction of the A and B parameters has been repeated for each region. Sample results are reported in Table 1 and Table 2 for p+ doped strained SiGe and p+ doped relaxed silicon.

Table 1: BTBT parameters for p++ strained $Si_{0.5}Ge_{0.5}$ on Si including BGN for N_{Dop} =2·10^{20} cm^{-3}.

Val. Valley	Cond. Valley	E_G [eV]	χ [eV]	A [10^{14} cm^{-3} s^{-1}]	B [MV/cm]
Γ_{hh}	Δ_{100}	0.52	4.35	7.85	8.81
Γ_{hh}	Δ_{010}	0.52	4.35	7.85	8.81
Γ_{hh}	Δ_{001}	0.84	4.03	4.60	15.88
Γ_{lh}	Δ_{100}	0.60	4.35	6.07	10.89

Γ_{lh}	Δ_{010}	0.60	4.35	6.07	10.89
Γ_{lh}	Δ_{001}	0.91	4.03	3.88	18.21

Table 2: BTBT parameters for p++ relaxed Si including BGN for N_{Dop} =2·10^{20} cm^{-3}.

Val. Valley	Cond. Valley	E_G [eV]	χ [eV]	A [10^{14} cm^{-3} s^{-1}]	B [MV/cm]
Γ_{hh}	Δ_{100}	0.93	4.16	8.26	27.13
Γ_{hh}	Δ_{010}	0.93	4.16	8.26	27.13
Γ_{hh}	Δ_{001}	0.93	4.16	13.18	22.50
Γ_{lh}	Δ_{100}	0.93	4.16	17.37	20.15
Γ_{lh}	Δ_{010}	0.93	4.16	17.37	20.15
Γ_{lh}	Δ_{001}	0.93	4.16	22.97	18.02

3.2 Calibration results

The simulation results for the homo-junction device of Figure 5 are reported in Figure 7 and Figure 8 using respectively the default S-Device calibration and the one performed on the k·p results. In both cases, the strong ambipolarity is not reproduced. This is probably due to inaccurate knowledge of the device structure and it would probably require a much more detailed knowledge of the drain/channel interface (doping profile, overlap/underlap, fringing field). On the other hand, the region of operation dominated by source/channel BTBT is well reproduced by the model calibrated on k·p, whereas the default calibration strongly overestimates the current. As explained in [Kao12] the linear interpolation of the BTBT parameters between Si and Ge in the defaults model predicts a too large BTBT generation rate since the model erroneously associates the high BTBT rate in Ge to phonon-assisted transitions, whereas direct ones are dominant under these circumstances. In this respect, SiGe essentially behaves as a silicon-like material, see also [Rev13].

Results for the hetero-junction device of Figure 6 are reported in Figure 9 and Figure 10 using respectively the default S-Device calibration and the one performed based on the k·p results. Again, ambipolarity is not reproduced. In the region of operation dominated by source/channel BTBT the k·p calibrated model works quite well. Also the default model is still close to the experiments; in fact, due to the low doping of the Si layer below the p+ SiGe, most of tunnelling path is in this Si layer (see Figure 11). The effect of the hetero-junction on the tunnelling barrier is captured by the default calibration, whereas the tunnelling masses are essentially those of the silicon layer.

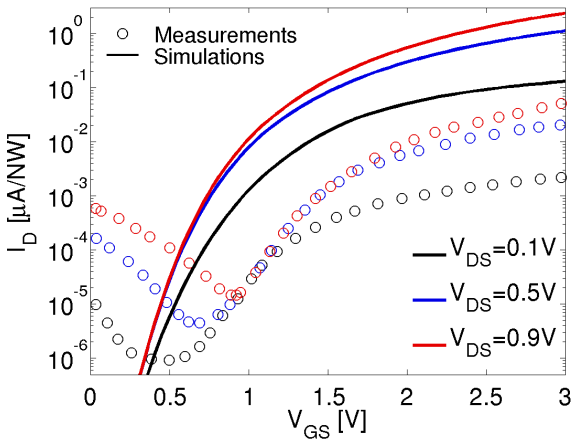

Figure 7: Simulated trans-characteristics for the homo-junction device with default S-Device BTBT parameters.

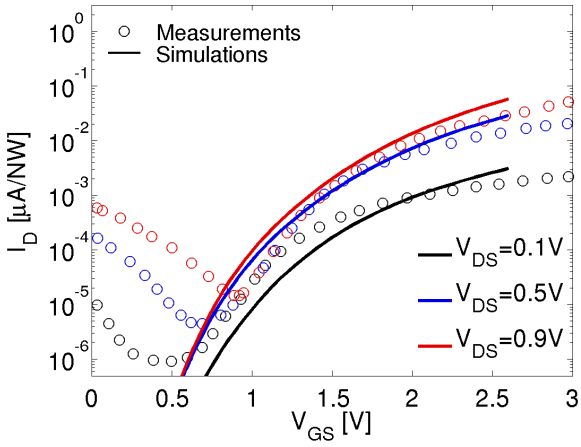

Figure 8: Simulated trans-characteristics for the homo-junction device with BTBT parameters from 30 band k•p.

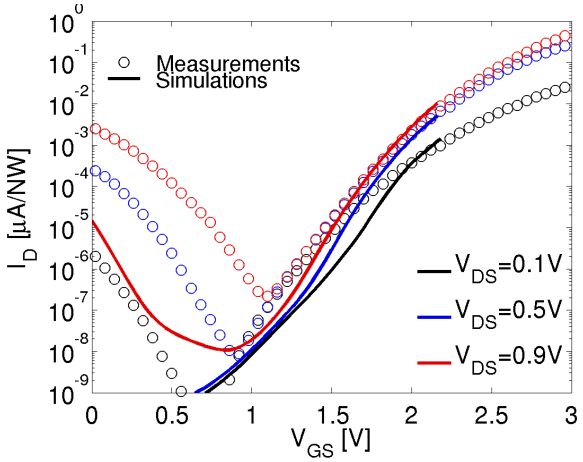

Figure 9: Simulated trans-characteristics for the hetero-junction device with default S-Device BTBT parameters.

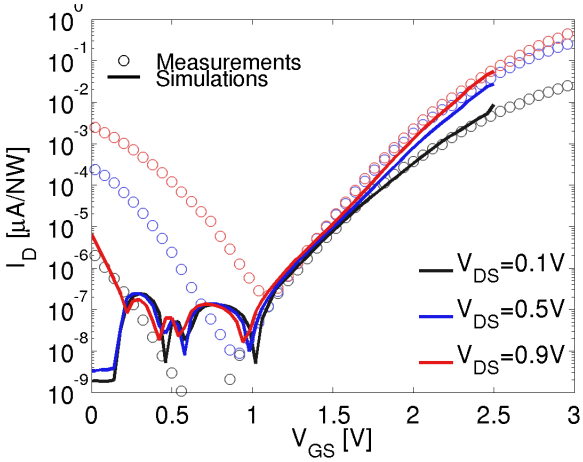

Figure 10: Simulated trans-characteristics for the hetero-junction device with BTBT parameters from 30 band k•p.

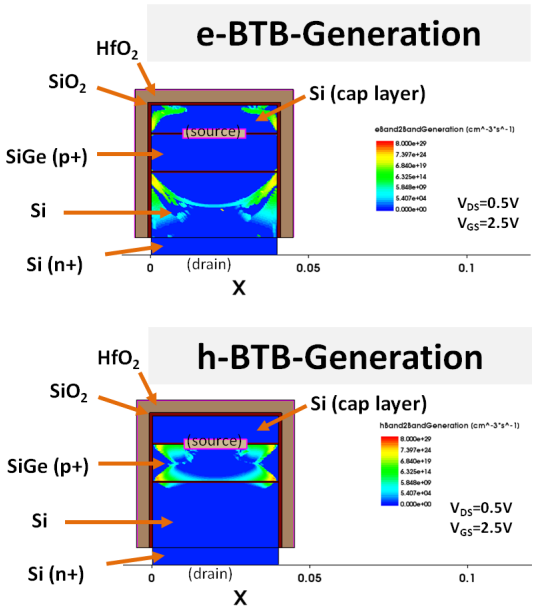

Figure 11: Map of the electron (top) and hole (bottom) generation rate along a vertical cut of the device in Figure 6.

One of the limitations of the 30 band k·p is that the E-k relationship cannot be computed inside the gap. For that reason, the electron and hole effective masses needed in the computation of the A and B terms of the dynamic non-local path BTBT model were extracted at the bottom of the conduction band and at the top of the valence band, respectively. We have then used the tool S-Band (included in the TCAD Sentaurus) to verify that for indirect gap materials such as Si and SiGe the effective mass extracted in the conduction/valence band is very similar to the one from the complex E-k inside the gap. Results are reported in Table 3 and Table 4 for silicon and strained SiGe, respectively. We see that the masses of the real and imaginary E-k are very close to each other. Note the anti-crossing of the valence band: the heavy and hole band are swapped into the gap (the imaginary branch of the heavy holes inside the gap has the same mass of the light hole branch in the valence band, and vice versa).

Table 3: Effective masses (in units of m_0) extracted with S-Band in the conduction/valence bands (real) or inside the gap (imag). Relaxed silicon. Different valleys and orientations are considered.

	[100]		[110]		[111]	
	Real	Imag	Real	Imag	Real	Imag
Δ_{100}	0.9142	0.9136	0.3227	0.3213	0.2438	0.2423
Δ_{010}	0.1959	0.1923	0.3227	0.3187	0.2438	0.2431
Δ_{001}	0.1959	0.1883	0.1959	0.1915	0.3227	0.3193
Γ_{hh}	0.2733	0.2044	0.5483	0.1453	0.6465	0.1398
Γ_{lh}	0.1991	0.3031	0.1458	0.6840	0.1401	0.7007

Table 4: Same as Table 3 but for strained $Si_{0.5}Ge_{0.5}$ on silicon.

	[100]		[110]		[111]	
	Real	Imag	Real	Imag	Real	Imag
Δ_{100}	0.8980	0.6660	0.3174	0.3055	0.2535	0.2522
Δ_{010}	0.1928	0.1789	0.3174	0.2822	0.2535	0.2387
Δ_{001}	0.1913	0.1668	0.1913	0.1750	0.3210	0.2833
Γ_{hh}	0.1558	0.1929	0.1557	0.1762	0.1909	0.2249
Γ_{lh}	0.1678	0.2152	0.1677	0.2053	0.1933	0.2381

3.3 Future work

We have shown that the calibration based on k·p results significantly improves the matching with the experiments compared to the default calibration. More extensive simulations with more accurate description of the devices are needed to better reproduce the ambipolarity. Also, data vs. temperature should be analysed and the contribution of trap-assisted tunnelling needs to be assessed (for example by comparison with pulsed measurements). The implications of anti-crossing need to be assessed.

4 TCAD tool Sentaurus-Device calibrated on S-Band (Synopsys)

This section describes the parameter calibration for Kane's two-band model provided by Sentaurus-Device of Synopsys on computations of pseudo-potential parameters with the tool S-Band of Synopsys. The pseudo-potential calculations to obtain band structure quantities of the group-IV element alloys, Si, Ge, and Sn are explained in detail. The application in 3D simulation of SiGe/Si TFETs fabricated by the project partner FZJ (Jülich) is demonstrated.

4.1 Pseudopotential calculations of group-IV (Si, Ge, and Sn) alloys

The nonlocal Empirical Pseudo-potential Method (EPM) parameters used for the band structure calculations are shown in Table 5. Pseudo-potential parameters of Sn were extracted with S-Band [SBa] by fitting the calculated band energies at symmetry points to the experimental data [San14]. A comparison of the calculated and experimental band energies and effective mass values is given in Table 6. The energies calculated in this work are similar to those given in [Che76]. The calculated energies associated with the direct and indirect band gaps (Γ_{7c} and L_{6c1}) agree well with the experimental data. The spin-orbit splitting calculated in this work is smaller than the experimental value. The parameters for Si and Ge were taken from [San13]. The band structures of GeSn and SiGeSn were calculated by employing the Virtual Crystal Approximation (VCA). The local pseudo-potential parameters of the alloy of any given composition were obtained by linearly interpolating the local pseudo-potential parameters of the individual atoms. The variation of lattice constants of GeSn and SiGeSn with the alloy composition was modelled using quadratic expressions fitted to the experimental lattice constants.

Table 5: EPM parameter values for Si, Ge, and Sn. Parameter values of Si and Ge were taken from [San13].

Parameter	Unit	Si	Ge	Sn
$V_{loc}(\sqrt{3})$	Ry	-0.2307	-0.2378	-0.21
$V_{loc}(\sqrt{8})$	Ry	0.0518	0.02852	0.02359
$V_{loc}(\sqrt{11})$	Ry	0.06878	0.0469	0.01739
α_0	Ry	0.02815	0.0	0.0
β_0	1	0.0	0.0	0.0
R_0	Angstrom	1.0599	0.0	1.0
α_2	Ry	0.0	0.309	0.71
R_2	Angstrom	0.0	1.2788	1.453
μ	Ry	0.00018	0.000965	0.00239
ξ	$\frac{1}{r_{\mathrm{Bohr}}}$	4.6	5.34	3.97
q^2 cutoff		11.5	12.44	15.25
Nonlocal Well		Square	Square	Square

The calculated direct and indirect band energies for GeSn are shown in Figure 12(a) and Figure 12(b), respectively. They are in excellent agreement with the experimental values at 300K. The measured values of the indirect band gap of GeSn have been extracted at 10K. Here, they are interpolated to 300K by using Varshni's law for the temperature dependence of the indirect band gap. The values of α and β for elemental Ge are used for the interpolation. The calculations suggest that the indirect-to-direct crossover of the band gaps of GeSn alloy occurs at a Sn content of ≈ 10%. A zero band gap of the GeSn alloy is found at the Sn content of ≈ 25%. The direct and indirect band energies of $(Si_{0.8}Sn_{0.2})_xGe_{1-x}$ are plotted vs. x in Figure 12(c) along with the experimental data. The measured band gap values are somewhat scattered and show some deviation from the calculated energies at intermediate x. This discrepancy can be explained as follows. The experimental band gaps have been obtained by photoluminescence (PL) measurements. PL signals from direct gap transitions (Γ-valley CB →VB) dominate those from indirect gap transitions (L-valley CB →VB),

when both Γ- and L-valley CB minima differ by a small energy. As the direct gap increases relative to the indirect gap, the indirect gap transitions start dominating the PL signal. This would shift the PL peak position from the direct gap energy to the indirect gap energy. In $(Si_{0.8}Sn_{0.2})_xGe_{1-x}$, the direct gap increases relative to indirect gap with increasing x. This may result in a gradual shift of the PL signal towards the indirect gap resulting in some deviation at intermediate x. It is interesting to note that a good reproduction of the experimental data is achieved without employing bowing of the EPM parameters. In this way, the pseudo-potential parameter set given in Table 5 can be used to calculate the band structure of SiGeSn that is in reasonable agreement with the experimental data.

Table 6: Comparison of the band energies at symmetry points calculated by EPM with the experimental band energies and the band energies calculated in Ref. [Che76]. The energies are given relative to the valence band edge ($\Gamma_{8c,v}$) of Sn.

Symmetry Points	Units	This Work	Ref.	Experimental
Γ_{6c}	eV	1.83	2.15	--
$\Gamma_{8c,v}$	eV	0.0	0.0	0.0
Γ_{7c} (Eg)	eV	-0.448	-0.41	-0.42
Γ_{6v} (SO)	eV	-0.66	-0.8	-0.8
L_{6c1}	eV	0.096	1.4	0.094
L_{6c2}	eV	3.22	3.48	-
$L_{4,5v}$	eV	-1.34	-1.2	-
L_{6v}	eV	-1.75	-1.68	-
X_{5c}	eV	1.04	0.9	
m_{LH} <100>	m_0	0.04	-	-
m_{HH} <100>	m_0	0.151	-	0.19

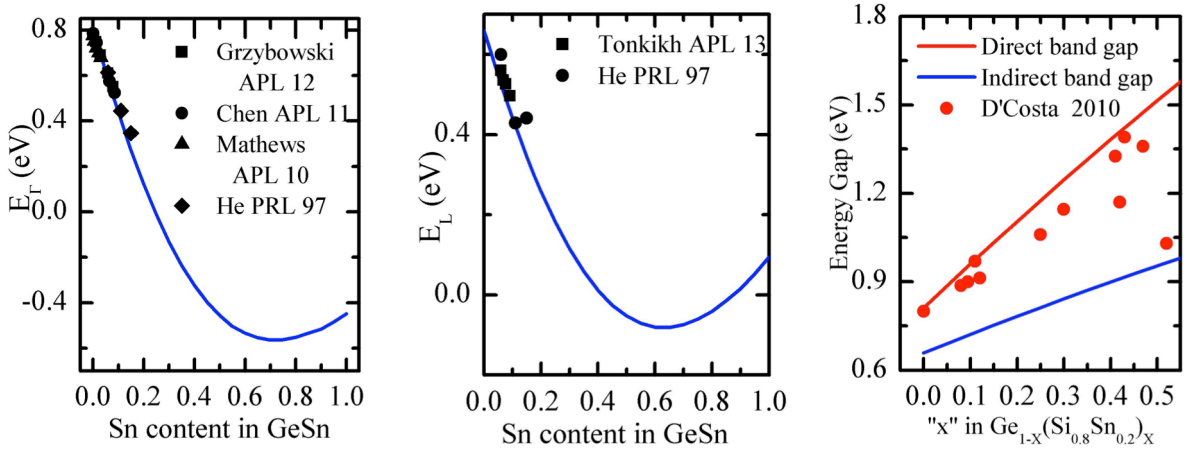

Figure 12: Comparison of experimental and calculated values of (a) direct band gap in GeSn, (b) indirect band gap in GeSn and (c) direct and indirect band gaps in SiGeSn.

4.2 Simulation of hetero-structure tunnel FETs

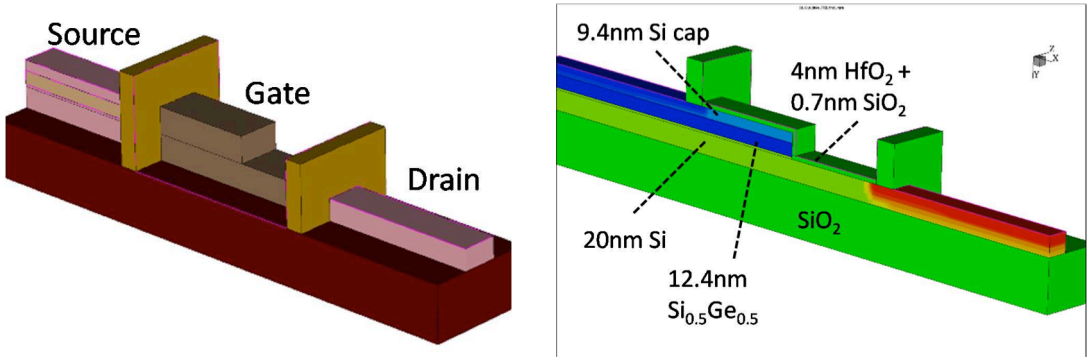

(a) (b)

Figure 13: (a) Device structure of $Si_{0.5}Ge_{0.5}$/Si hetero-junction nanowire-TFET simulated using 3D simulations. (b) A vertical cut along the plane of symmetry. It shows the doping profiles and the structure of the TFET.

The EPM was applied to obtain the band structure quantities for the BTBT model of S-Device [SDe] to be used in 3D simulations of the same $Si_{0.5}Ge_{0.5}$/Si hetero-structure TFET [Ric13] as already presented in Section 3.1.2. The TFET has the form of a lateral nanowire etched from Si-cap/p++ $Si_{0.5}Ge_{0.5}$ /n-Si hetero-structures grown over SiO_2. Etching the nanowires down to Si at one end results in a step-like structure as shown in Figure 13. The gate stack contains a 4 nm thick HfO_2 layer in addition to a ~ 0.7 nm native oxide (total EOT = ~ 1.4 nm). The "dynamic non-local path BTBT model" and the Shockley-Read-Hall (SRH) generation-recombination model were employed in the simulations. The parameters used for the BTBT model are listed in Table 7. The major contribution to the BTBT current comes from under-the-gate tunnelling ("line tunnelling") in the SiGe layer along the vertical side-walls which necessitates 3D simulations. As the device dimensions are too big for 3D simulations, a shorter device with 100 nm gate-source overlap instead of 2 µm overlap was simulated. The simulated drain current was multiplied by 20 to obtain the actual drain current shown in the figures. The simulated I_D-V_G characteristics of the device are in good agreement with the experimental I_D -V_G curves (Figure 14(a)) after adjusting the gate work function (i.e. increasing it from 4.25 eV to 5.1 eV). A large shift in the work function suggests quantization in the channel region which results in delayed turn-on. The slight underestimation of I_D at low V_G in the simulation is attributed to trap-assisted tunnelling due to the defects present both at the SiGe/Si as well as the HfO_2 /SiGe interface (not modelled). The simulated I_D-V_D curves (Figure 14(b)) show qualitative resemblance, although the current values differ significantly. The SiGe layer was assumed to be fully relaxed in calculating the BTBT parameters. Presence of strain in the layer doesn't change the sub-threshold characteristics much but reduces the on-state current as can be seen in Figure 14(c). In this way, the device simulations yield a reasonable match with the experiments when the band structure quantities obtained from the EPM calculations described above are used as inputs to the BTBT model [San14].

Table 7: Band structure quantities required to model BTBT in a $Si_{0.5}Ge_{0.5}$/Si hetero-TFET.

Parameter	Unit	$Si_{0.5}Ge_{0.5}$		Si	
		Direct	Indirect	Direct	Indirect
E_g	eV	-	0.984	-	1.106
m_C<100>	m0	0.103	0.194	0.405	0.198
m_{LH}<100>	m0	0.125	0.125	0.189	0.189
Degeneracy	1	2	8	2	8
gD_{op}^2/ρ	J^2mkg^{-1}	-		-	3.54e-21
Δ_C	eV	1.355		2.251	
ϵ_{op}	meV	-	13.8	-	19.0

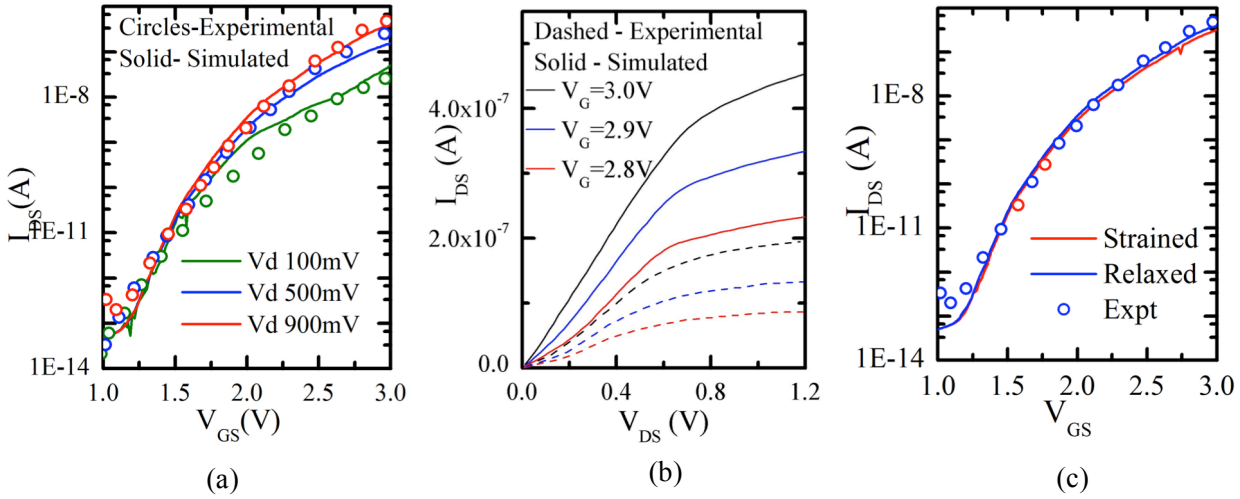

Figure 14: Results of 3D simulations of the TFET shown in Fig. 13. (a). Comparison of simulated and experimental I_{DS} –V_{GS} characteristics, and (b) I_{DS} -V_{DS} characteristics of the device. The parameters for a fully relaxed SiGe layer on Si were used in the simulations (listed in Table 7). (c). Comparison of simulated I_{DS} -V_{GS} characteristics by assuming either strained or relaxed SiGe layer.

4.3 Future work

The developed pseudo-potential parameter set and the workbench can provide the band structure quantities for SiGeSn alloys of any arbitrary composition. These quantities can be used to simulate the GeSn/SiGeSn hetero-tunnel FETs for a wide range of alloy compositions. The simulation results can then be used to determine the optimum alloy composition(s) for GeSn/SiGeSn hetero-tunnel FET applications.

5 Conclusion

Modeling TFETs using the "dynamical nonlocal path BTBT" (Kane two-band model) implemented in Sentaurus-Device requires a number of band structure parameters such as DOS, band offsets, direct and indirect band gaps, and effective masses for the given semiconductors. S-Device serves as the work horse in the project because realistic device structures are too large for ad-hoc simulators and because all dissipative effects as well as additional generation-recombination rates can be included. Rigorous band structure calculations have to be performed to extract such quantities. Various ways are available to do so, such as the k·p method, TB, EPM, and others. We have described the validation of OMEN and did extensive calibrations of the TCAD parameters by 30 band k·p and by EPM calculations. Of particular value are TCAD calibrations by comparison with OMEN results, which can be based on short (ballistic) homo- and hetero Esaki diodes. For this, one has to suppress the dissipative effects in S-Device. In the case of InAs-Si hetero-junctions it was found that the inter-material tunnelling is a direct (zero-phonon) process. Two TCAD variants have been discussed to match this case. Comparison with OMEN also allows to study the effect of quantization and strain. It has to be mentioned, however, that various uncertainties remain. The work function is a fitting parameter, and the band gap is influenced by band gap narrowing. In the case of size quantization, two available quantum-correction models can be activated in S-Device simulations, but the consequences on the used parameters are still to be investigated.

In summary, we obtained a TCAD BTBT parameter set for all materials, material combinations, and compositions relevant for the project. This also includes future TFETs to be fabricated at IBM (III-V on Si, all-III-V) and at FZJ (GeSn on SiGeSn). In the further course of the project, the calibration results can be used to determine the optimum alloy composition(s) for ternary-III-V/Si, ternary-III-V/III-V, and GeSn/SiGeSn hetero-TFETs. The methods are suitable to calibrate BTBT parameters for strained materials and for strained hetero-junctions. This enables the simulation of an extended design space including strain.

References

[Lui06] M. Luisier, A. Schenk, W. Fichtner, and G. Klimeck, *Phys. Rev. B* **74**, 205323 (2006).

[MLu09] M. Luisier and G. Klimeck, *IEEE Elec. Dev. Lett*. 30, p. 602, 2009.

[Lui10] M. Luisier and G. Klimeck, *J. Appl. Phys*. 107, 084507, 2010.

[Lui09] M. Luisier and G. Klimeck, *Proc.* IEDM 2009, pp. 913 – 916.

[Aga10] S. Agarwal, G. Klimeck, and M. Luisier, *IEEE Elec. Dev. Lett*. 31, pp. 621-623, 2010.

[Cho12] W.-S. Cho et al., *Appl. Phys. Lett*. 100, 063504, 2012.

[Lak97] R. Lake, G. Klimeck, R. C. Bowen, and D. Jovanovic, *J. Appl. Phys. 81*, 7845 (1997).

[LuK09] Luisier and G. Klimeck, *Phys. Rev. B* 80, 155430 (2009).

[Jan98] J.-M. Jancu, R. Scholz, F. Beltram, and F. Bassani, *Phys. Rev. B* 57, 6493, 1998.

[Boy02] T. B. Boykin, G. Klimeck, R. Chris Bowen, and F. Oyafuso, *Phys. Rev. B*, 66, 125207, 2002.

[Boy04] T. B. Boykin, G. Klimeck, and F. Oyafuso, *Phys. Rev. B* 69, 115201, 2004.

[Lee04] S. Lee, F. Oyafuso, P. von Allmen, and G. Klimeck, *Phys. Rev. B* 69, 045316, 2004.

[ioffe] http://www.ioffe.rssi.ru/SVA/NSM/Semicond/

[Paw12] D. Pawlik et al., IEEE International Electron Devices Meeting (IEDM), 2012, DOI: 10.1109/IEDM.2012.6479118.

[Sch12] A. Schenk et al., 70th Device Research Conference (DRC), Penn-State, June 18-20, pp. 201-202, 2012.

[Nun14] H. Carrillo-Nunez et al., *Proc*. ESSDERC 2014, to be published

[Sol04] P. M. Solomon et al., *J. Appl. Phys*., vol. 95, 5800, 2004.

[SDe] Sentaurus-Device User Guide, Version 2013.03, Synopsys Inc., Mountain View, California, 2013.

[Rid06] D. Rideau et al., *Phys.Rev. B* **74**, 195208 (2006).

[Liz12] D. Lizzit et al., *Proc.* ESSDERC 2012, p.322

[Jai90] S. C. Jain et al., Jour. Appl. Phys., vol. 68, p. 3747–3749, 1990.

[Rev13] A. Revelant et al., *Proc.* ESSDERC 2013, p.49

[Ric13] S. Richter et al., *Proc.* ULIS 2013, p.25

[Kao12] K.-H. Kao et al. Trans. on Electron Devices, vol. 59, p. 292 , 2012.

[SBa] Sentaurus Device Monte Carlo User Guide, Version 2013.03, Synopsys Inc., Mountain View, California, 2013.

[San14] S. Sant, Q. T. Zhao, D. Buca, S. Mantl, and A. Schenk, "Analysis of GeSn-SiGeSn Hetero-Tunnel FETs," in Proc. SISPAD, Yokohama, 2014.

[Che76] J. R. Chelikowsky and M. L. Cohen, *Phys. Rev*. B., vol. 14, pp. 556-582, 1976.

[San13] S. Sant et al., *J. Appl. Phys*., vol. 113, p. 033708, 2013.